

Formation of a partially-screened inner acceleration region in radio pulsars: drifting subpulses and thermal X-ray emission from polar cap surface

Janusz Gil^{1,2}, George Melikidze^{1,3} & Bing Zhang ²

Received _____; accepted _____

¹Institute of Astronomy, University of Zielona Góra, Lubuska 2, 65-265, Zielona Góra, Poland

²Department of Physics, University of Nevada, Las Vegas, USA

³CPA, Abastumani Astrophysical Observatory, Al. Kazbegi ave. 2a, 0160, Tbilisi, Georgia

ABSTRACT

Formation of a partially-screened inner acceleration region in 102 pulsars with drifting subpulses is considered. This is motivated by that spark discharges leading to drifting subpulses cannot be produced in a steady polar cap flow and thus the inner accelerator should be intermittent in nature, that the traditional pure vacuum gap model predicts too fast a sub-pulse drifting rate, and that recent X-ray observations as well as the radio drifting data are both consistent with the inner gap being partially screened. By means of the condition $T_c/T_s > 1$ (where T_c is the critical temperature above which the surface delivers a thermal flow to adequately supply the corotation charge density, and T_s is the actual surface temperature), it is found that a partially-screened acceleration region can be formed given that the near surface magnetic fields are very strong and curved. We consider both curvature radiation (CR) and resonant inverse Compton scattering (ICS) to produce seed photons for pair production. It is found that the ICS mechanism is unlikely to develop a partially screened gap, while the CR mechanism can naturally drive the sparking discharge of such a gap. Observational signatures of thermal radiation from the spark-heated polar caps are consistent with the model that invokes a partially screened gap formed in strong nondipolar surface magnetic fields.

Subject headings: pulsars: general — stars: neutron — X-rays: stars

1. Introduction

The phenomenon of drifting subpulses is a long standing puzzle in the pulsar research. It is generally believed that this phenomenon is inherently associated with the so-called inner acceleration region above the polar cap, in which the magnetospheric plasma does not corotate with the neutron star surface. The first model based on this idea was proposed by Ruderman & Sutherland (1975, RS75 henceforth). The predictions of RS75 model were successfully compared with just a few pulsars known to show this phenomenon at that time. A decade later, Rankin (1986, R86 hereafter) compiled a list of about 40 drifting pulsars, but drifting subpulses were still regarded as some kind of exceptional phenomenon. However, recently Weltevrede, Edwards, & Stappers (2006, WES06 hereafter) presented the results of a systematic, unbiased search for subpulse modulation in 187 pulsars and found that the fraction of pulsars showing drifting subpulse phenomenon is likely to be larger than 55%. They identified 102 pulsars with drifting subpulses in their sample, with a large fraction of newly discovered drifters. The authors concluded that the conditions required for the drifting mechanism to work cannot be very different from the emission mechanism of radio pulsars. WES06 then suggest that the subpulse drifting phenomenon is an intrinsic property of the pulsar emission mechanism, although drifting could in some cases be very difficult or even impossible to detect due to the low signal-to-noise ratio. It is therefore essential to attempt unravelling the physical conditions that can lead to formation of an inner acceleration region above the polar cap that could lead to development of the subpulse drift phenomenon.

The classical vacuum gap model of RS75 (in which sparks-associate sub-beams of subpulse emission circulate around the magnetic axis due to $\mathbf{E} \times \mathbf{B}$ drift of spark plasma filaments) provides the most natural and plausible explanation of drifting subpulse phenomenon. However, despite its popularity, this model suffers from the so-called binding

energy problem, i.e. the surface charges (ions or electrons) are likely to be directly pulled out of the surface so that a pure vacuum gap is difficult to form. However, the steady flow polar cap models, the so-called space-charge-limited flow models (Arons & Scharlemann 1979; Harding & Muslimov 1998), cannot give rise to the intermittent “sparking” behavior, which is likely a common ingredient of the inner accelerator models in view of the prevalence of the sub-pulse drifting phenomenon in radio pulsars. Gil & Mitra (2001, GM01 hereafter) revisited the binding energy problem of the RS75 model and argued that the formation of the vacuum gap (VG) is, in principle possible, although it requires a very strong surface magnetic fields, much stronger than a dipolar components inferred from the observed spindown rate. It has been known for a long time that in order to allow all radio pulsars to produce electron-positron pairs (the necessary condition for coherent radio emission), the near-surface magnetic fields must include multipole components (Ruderman & Sutherland 1975; Arons & Scharlemann 1979; Zhang, Harding, & Muslimov 2000). However, GM01 argued that in general, the surface magnetic field at the polar cap could be significantly nondipolar. It seems that there is growing observational evidence of nondipolar structure of surface magnetic field, and the suggestion to form such sunspot-like fields during the early proto neutron star stage has been proposed (e.g. Urpin & Gil 2004). Gil & Melikidze (2002, GM02 hereafter) developed further this idea and calculated the VG model for 42 pulsars tabulated by R86. Using different pair production mechanisms and different available estimates of the cohesive energy of surface iron ions, GM02 argued that VGs can be formed for all pulsars from R86 and that under pure vacuum gap condition the magnetic pair production should be dominated by resonant ICS seed photons.

Although the binding energy problem can be resolved by assuming an appropriately strong surface magnetic field, yet another difficulty of the RS75 model is that it predicted a much too fast $\mathbf{E} \times \mathbf{B}$ drift rate. Motivated by this issue Gil, Melikidze, & Geppert (2003, GMG03 hereafter) developed further the idea of the inner acceleration region above the

polar cap by including the partial screening by a sub-Goldreich-Julian thermal flow from the surface due to polar cap heating by the sparks (Cheng & Ruderman 1980, CR80 henceforth). They managed to construct a self-consistent model, which was successfully applied to several well known drifters for which the intrinsic drift rate (sometimes called the carousel rotation time) was measured or estimated. In this paper we call such an inner accelerator a partially screened gap (PSG henceforth). The latest XMM-Newton observation of the drifting pulsar PSR B0943+10 (Zhang, Sanwal, & Pavlov 2005, ZSP05 hereafter) reveals a possible hot spot with a surface area much smaller than the conventional polar cap, which is consistent with the origin of polar cap heating from such a PSG that can give the right subpulse drifting rate. This lends strong support to the PSG model. In this paper we apply the PSG model to a new set of 102 pulsars from WES05 and show that it can work in every case, provided that the surface non-dipolar magnetic field is strong enough, even stronger than 10^{13} G suggested by GM02 and GMG03. Our new treatment is a combination of those used in GM02 and GMG03. Unlike in the pure VG case considered by GM02, we demonstrate that in the PSG model developed by GMG03 the ICS is no longer the dominating mechanism of magnetic pair production.

Our starting hypothesis is that the drifting subpulses manifest the existence of an inner acceleration region that discharges in a quasi-steady manner via a number of $\mathbf{E} \times \mathbf{B}$ drifting sparks¹. Within the sparking gap model, the intrinsic (non-aliased) subpulse drift rate and the polar cap heating rate (manifested as the thermal X-ray luminosity) should be correlated with each other, since they are determined by the same value of the accelerating potential drop. In an accompanying paper, Gil, Melikidze & Zhang (2006, hereafter Paper

¹Other suggestions of subpulse drifting have been made (e.g. Wright 2003), but the connection between the radio drifting rate and the X-ray properties in those models is not yet clear, and we do not discuss them in the current paper.

I) found a specific relationship between the appropriate observables and concluded that it holds for a number of pulsars for which good quality data is available (especially PSR B0943+10, Zhang et al. 2005). It turns out that this relationship depends only on the observables and thus it is a powerful tool for testing different theoretical models. Although the number of pulsars that have all necessary data for such testing is small at the moment, the clean prediction holds the promise to ultimately confirm (or discard) the PSG model in the future. In this paper we analyze this model in a more detailed manner to investigate the microscopic conditions (e.g. near-surface configuration, radiation mechanism, etc) that are needed to form such PSGs.

2. Charge depleted inner acceleration region

The inner acceleration region above the polar cap results from the deviation of a local charge density ρ from the co-rotational charge density (Goldreich & Julian 1969, GJ69 hereafter)

$$\rho_{\text{GJ}} = -\frac{\Omega \cdot \mathbf{B}_s}{2\pi c} \approx \pm \frac{B_s}{cP}, \quad (1)$$

where the positive/negative sign corresponds to $^{56}_{26}\text{Fe}$ ions/electrons. These two possibilities correspond to antiparallel and parallel relative orientation of the magnetic and spin axes, respectively. As mentioned before, there exists growing evidence (see Urpin & Gil 2004, and references therein) that the actual surface magnetic field B_s is highly non-dipolar. Its magnitude can be described in the form

$$B_s = bB_d \quad (2)$$

(Gil & Sendyk 2000, GS00 hereafter), where the enhancement coefficient $b > 1$ and

$$B_d = 2 \times 10^{12} (P\dot{P}_{-15})^{1/2} \text{ G} \quad (3)$$

is the canonical, star centered dipolar magnetic field, P is the pulsar period in seconds and $\dot{P}_{-15} = \dot{P}/10^{-15}$ is the period derivative.

The polar cap is defined as the locus of magnetic field lines that penetrate the light cylinder (GJ69). Generally, the polar cap radius can be written as

$$r_p = 1.45 \times 10^4 P^{-0.5} b^{-0.5} \text{ cm} \quad (4)$$

(GS00), where the factor $b^{-0.5}$ describes squeezing of the polar cap area due to the magnetic flux conservation in non-dipolar surface fields (as compared with the GJ69 dipolar configuration).

Charge depletion in the acceleration region above the polar cap can result from binding of the positive $^{56}_{26}\text{Fe}$ ions (at least partially) in the neutron star surface. Positive charges then cannot be supplied at the rate that would compensate the inertial outflow through the light cylinder. As a result, a significant part of the unipolar potential drop (GJ69, RS75) develops above the polar cap, which can accelerate charged particles to relativistic energies and power the pulsar radiation. The characteristic height h of such an acceleration region is determined by the mean free path of pair-producing high energy photons. In other words, the growth of the accelerating potential drop is limited by the cascading production of an electron-positron plasma (e.g. RS75, CR80). The accelerated positrons would leave the acceleration region, while the electrons would bombard the polar cap surface, causing a thermal ejection of ions, which are otherwise more likely bound in the surface in the absence of additional heating. This thermal ejection would cause partial screening of the acceleration potential drop ΔV corresponding to a shielding factor

$$\eta = 1 - \frac{\rho_i}{\rho_{\text{GJ}}}, \quad (5)$$

where ρ_i is thermonically ejected charge density and

$$\Delta V = \eta \frac{2\pi}{cP} B_s h^2, \quad (6)$$

where B_s is defined by equation (2) and h is the model dependent height of the acceleration region (see below). The above expression for ΔV is the solution of Poisson equation for a thin PSG, assuming that $\partial\eta/\partial h = 0$ within the acceleration region (see GMG03 for details).

The values of the shielding factor can be estimated observationally for pulsars with drifting subpulses as $\eta = (1/2\pi)(P/P_3)$, where P_3 is the primary drift periodicity (Eq.[A2] in Paper I). Since typically P_3/P is typically several (R86, WES05), in general the shielding factor η is likely much smaller than unity. It means that the conditions within the actual acceleration region above the polar cap should greatly differ from the pure vacuum gap proposed by RS75.

Following the original suggestion by CR80, GMG03 argued that because of the exponential sensitivity of the accelerating potential drop ΔV to the surface temperature T_s , the actual potential drop should be thermostatically regulated. In fact, when ΔV is large enough to ignite the cascading pair production, the backflowing relativistic charges will deposit their kinetic energy in the polar cap surface and heat it at a predictable rate. This heating will induce thermionic emission from the surface, which will in turn decrease the potential drop that caused the thermionic emission in the first place. As a result of these two oppositely directed tendencies, the quasi-equilibrium state should be established, in which heating due to electron bombardment is balanced by cooling due to thermal radiation. This should occur at a temperature T_s slightly lower than the critical temperature above which the polar cap surface delivers thermionic flow at the corotational (GJ69) charge density level (see GMG03 for more details).

The quasi-equilibrium condition is $\sigma T_s^4 = \gamma m_e c^3 n$, where $\gamma = e\Delta V/m_e c^2$ is the Lorentz factor and ΔV is the accelerating potential drop (Eq. [6]), $n = n_{\text{GJ}} - n_i = \eta n_{\text{GJ}}$ is the charge number density of back-flowing particles that actually heat the polar cap surface, η is the shielding factor (Eq. [5]), n_i is the charge number density of thermally ejected flow

and $n_{\text{GJ}} = \rho_{\text{GJ}}/e = 1.4 \times 10^{11} \dot{P}_{-15}^{0.5} P^{-0.5} b \text{ cm}^{-3}$ (Eq. [1]) is the corotational (GJ69) charge number density. It is straightforward to obtain an expression for the quasi-equilibrium polar cap surface temperature in the form

$$T_s = (2 \times 10^6 \text{ K}) P^{-0.25} \dot{P}_{-15}^{0.25} \eta^{0.5} b^{0.5} h_3^{0.5}, \quad (7)$$

where $h_3 = h/10^3 \text{ cm}$ is the normalized height of the acceleration region. This height is model dependent and we discuss two possible models below (Eqs. [9] or [10]). Growing evidence suggests that in actual pulsars T_s is few MK (see Table 1 in Paper I and references therein). Thus, from the above equation one can infer that $b \sim \eta^{-1}$, where the shielding parameter should be much lower than unity (see discussion below Eq. [6]). As a consequence, the enhancement coefficient $b = B_s/B_d$ (Eq. [2]) should be much larger than unity (at least of the order of 10). This is very consistent with the binding energy problem discussed in Section 3.

The predicted thermal X-ray emission luminosity from the polar cap with temperature T_s is $L_x = \sigma T_s^4 A_{\text{bol}}$, where $A_{\text{bol}} = \pi r_p^2$ and r_p is the actual polar cap radius (Eq. [4]) and σ is the Stefan-Boltzmann constant. Since $T_s \approx (2-3) \times 10^6 \text{ K}$ (see Table 1 in Paper I) then $L_x = (6-30) \times 10^{29} b^{-1} P^{-1} \text{ erg/s}$. When this is compared with observational values, which are usually well below 10^{29} erg/s , one can conclude that $b > 10$, in agreement with the estimate given above.

RS75 derived a famous formula for their VG height assuming that the quasi-steady breakdown is driven by magnetic pair production induced by the curvature radiation seed photons. They used Erber (1966) approximation, which is valid in relatively low magnetic fields $B_s/B_q \lesssim 0.1$, where

$$\frac{B_s}{B_q} = 0.046 (P \dot{P}_{-15})^{0.5} b \quad (8)$$

and $B_q = 4.414 \times 10^{13} \text{ G}$ is the so-called quantum magnetic field. In the strong surface magnetic field, e.g. $B_s > 5 \cdot 10^{12} \text{ G}$, the high energy photons with energy $E_f = \hbar\omega$

produce electron-positron pairs at or near the kinematic threshold $\hbar\omega = 2mc^2/\sin\theta$, where $\sin\theta = l_{\text{ph}}/\mathcal{R}$, l_{ph} is the photon mean free path for pair formation and $\mathcal{R} = \mathcal{R}_6 \cdot 10^6$ cm is the radius of curvature of magnetic field lines. This regime is called the near threshold (NT) conditions (e.g. Daugherty & Harding 1983). Two VG models can be considered under the NT conditions: Curvature Radiation dominated Near Threshold Partially Screened Gap (CR-NTPSG) model and Inverse Compton Scattering dominated Near Threshold Partially Screened Gap (ICS-NTPSG) model, in which the potential drop is limited by pair production of the CR and the resonant ICS seed photons, respectively. Proper expressions corresponding to pure vacuum gap case have been derived by GM01 and GM02. Below we give generalized formulae by including partial screening due to the thermal flow from the polar cap surface (GMG03 and references therein).

CR-NTPSG model

In this model the cascading e^-e^+ pair plasma production is driven (or at least dominated) by the curvature radiation photons with typical energy $\hbar\omega = (3/2)\hbar\gamma^3c/\mathcal{R}$, where γ is the typical Lorentz factor of electrons/positrons moving relativistically along the local surface magnetic field lines with a radius of curvature \mathcal{R} . In the quasi-steady conditions the height h of the acceleration region is determined by the mean free path that is $h \sim l_{\text{ph}}$ for pair production by energetic CR photon in the strong and curved magnetic field. Following GM01 (see also GM02) and including the partial screening effect (GMG03) we obtain

$$h \approx h^{\text{CR}} = (3.1 \times 10^3)\mathcal{R}_6^{2/7}\eta^{-3/7}b^{-3/7}P^{3/14}\dot{P}_{-15}^{-3/14} \text{ cm.} \quad (9)$$

ICS-NTPSG model

In this model the cascading pair plasma production is driven (or at least dominated)

by the resonant inverse Compton scattering (e.g. Zhang et al. 1997), with typical photon energy $\hbar\omega = 2\gamma\hbar eB_s/mc$. In the quasi-steady conditions the height h of the acceleration region is determined by the condition $h \sim l_e$ where $l_e = 0.0027\gamma^2(B_s/10^{12}\text{G})^{-1}(T_s/10^6\text{ K})^{-1}$ is the mean free path of the electron to emit this high energy ICS photon (ZHM00), B_s is the surface magnetic field and T_s is the actual surface temperature. Following GM01 and including partial screening (GMG03) we obtain

$$h \approx h^{\text{ICS}} = (5 \times 10^3)\mathcal{R}_6^{4/7}\eta^{-1/7}b^{-1}P^{-5/14}\dot{P}_{-15}^{-1/2} \text{ cm.} \quad (10)$$

In the above equations $\mathcal{R}_6 = \mathcal{R}/10^6$ cm is the normalized curvature radius of the surface magnetic field lines. In the following discussion eqs. (9) and (10) will be referred as to CR and ICS cases, respectively.

3. Binding energy problem

If the binding energy of $^{56}_{26}\text{Fe}$ ions is large enough to prevent thermionic emission, a charge depleted acceleration region can be formed just above the polar cap. Normally, at the solid-vacuum interface, the charge density of outflowing ions is roughly comparable with density of the solid at the surface temperature $kT_s = \varepsilon_c$, where ε_c is the cohesive (binding) energy and $k = 8.6 \times 10^{-8}$ keVK $^{-1}$ is the Boltzman constant. However, in the case of pulsars, only the corotational charge density ρ_{GJ} can be reached, and the $^{56}_{24}\text{Fe}$ ion number density corresponding to ρ_{GJ} is about $\exp(-30)$ times lower than in the neutron star crust. Since the density of outflowing ions ρ_i decreases in proportion to $\exp(-\varepsilon_c/kT_s)$, one can then write $\rho_i/\rho_{\text{GJ}} \approx \exp(30 - \varepsilon_c/kT_s)$. At the critical temperature

$$T_i = \frac{\varepsilon_c}{30k} \quad (11)$$

the ion outflow reaches the maximum value $\rho = \rho_{\text{GJ}}$ (Eq. [1]), and the numerical coefficient 30 is determined from the tail of the exponential function with an accuracy of about 10%.

Calculations of binding energies are difficult and uncertain. In this paper we use the results of (Jones 1986, J86 henceforth), which were recommended by Lai (2001) in his review paper as more robust than others. J86 obtained $\varepsilon_c = 0.29, 0.60$ and 0.92 keV for $B_s = 2, 5$ and 10×10^{12} G, respectively. These values can be approximately represented by the function $\varepsilon_c \simeq (0.18 \text{ keV})(B_s/10^{12})^{0.7}$ G. Using equations (2), (3) and (11), this could be converted into the critical temperature

$$T_i \simeq (0.7 \times 10^5 \text{ K}) \left(\frac{B_s}{10^{12} \text{ G}} \right)^{0.7} \simeq (1.2 \times 10^5 \text{ K}) b^{0.7} (P\dot{P}_{-15})^{0.36} \approx (10^6 \text{ K}) \left(\frac{B_s}{B_q} \right)^{0.7}, \quad (12)$$

where we use the ratio B_s/B_q (Eq. [8]) for the convenience of presenting the results in the graphical form (Fig. 1 and 2). Above this temperature the thermionic ion flow reaches the maximum GJ density at the surface, and the polar cap flow will be space charge limited. An acceleration potential can be still developed but the growth rate is slow compared with the PSG model we are developing in this paper. At temperatures below T_i charge-depletion would happen right above the surface, and an efficient acceleration region would form, which should be discharged in a quasi-steady manner by a number of sparks, similar to the original suggestion of RS75 for the pure vacuum gap case (see more detailed discussion in GMG03). The electron-positron plasma produced by sparking discharges co-exists with the thermally ejected ions, whose charge density can be characterized by the shielding factor (defined by Eq. [5]) in the form

$$\eta = 1 - \exp \left[30 \left(1 - \frac{T_i}{T_s} \right) \right]. \quad (13)$$

As one can see from equations (5) and (13), at the temperature $T_i = T_s$ the shielding factor $\eta = 0$ (corresponding to fully developed space-charge limited flow with $\rho_i = \rho_{\text{GJ}}$), but even a very small drop of T_s below T_i , much smaller than 10%, corresponds to creation of the pure vacuum gap with $\eta = 1$ ($\rho_i = 0$). Thus, the condition for partially screened charge depleted acceleration region can be written in the form $T_s \lesssim T_i$, meaning that the actual surface

temperature T_s should be slightly lower (few percent) than the critical ion temperature T_i , which for a given pulsar is determined purely by the surface magnetic field B_s (Eq. [12]). Practically, one can use

$$T_s = T_i, \quad (14)$$

to denote the condition of forming a PSG, with the caveat that in reality T_s cannot be exactly equal to T_i but should be a few percent lower.

As mentioned above, the polar cap surface can be, in principle, negatively charged ($\Omega \cdot \mathbf{B} > 0$). In such a case (called “antipulsars” by RS75) the polar cap surface can deliver an electron flow. Following GMG03 we assume that this electron flow is also determined mainly by thermo-emission, with the corresponding shielding factor $\eta = 1 - \rho_e/\rho_{\text{GJ}} = 1 - \exp[25(1 - T_e/T_s)]$, where ρ_e is the charge density of thermionic electrons. The critical electron temperature is

$$T_e \simeq (5.9 \times 10^5 \text{ K}) b^{0.4} P^{0.16} \dot{P}_{-15}^{0.2} \sim (10^6 \text{ K}) \left(\frac{B_s}{B_q} \right)^{0.4} \quad (15)$$

(see GMG03 for more details), and in analogy to equation (14) the condition for creation of charge depleted acceleration region is $T_s = T_e$. Since the enhancement coefficient $b \gg 1$ (see the discussion following Eq. [7]) so that $B_s/B_q \sim 1$ (Eq. [8]), both T_i and T_e can be close to $T_s \sim$ a few MK. Since T_i and T_e are similar, we will only include the ion case (Eq. [12]) in the following discussion, keeping in mind that our considerations are general and independent of the sign of the polar cap charge, at least qualitatively.

4. Models of the inner acceleration region in pulsars

In this section we present calculation results similar to those presented by GM02 but for a much larger sample of drifting subpulse pulsars and with the inclusion of partial screening due to thermionic emission from the polar cap surface. The condition for the

formation of the gap used in GM02 was $T_c/T_s > 1$, while in this paper we used $T_c/T_s = 1$ (Eq. [14]) as a result of the thermostatic regulation considered by GMG03.

4.1. CR-NTPSG

The results of model calculations for 102 pulsars with drifting subpulses (see Table 1) are presented in Fig. 1 for the ion T_i critical temperature (Eq. [12]). We have plotted B_s/B_q (left-hand side vertical axes) versus the pulsar number (which corresponds to a particular pulsar according to Table 1). The actual value of B_s/B_q (Eq. [8]) for a given pulsar was computed from the condition $T_s = T_i$, where T_s is the actual surface temperature (Eq. [7]), with the height h of CR driven acceleration region determined by equation (9). This condition leads to the expression $B_s/B_q = 126.4P^{-20/29}\mathcal{R}_6^{10/29}\eta^{20/29}$, which allows to sort pulsars according to decreasing value of pulsar period P , which is marked on the top of the Figure 1. The vertical axes on the right hand side are expressed in terms of the surface temperature T_s computed from equation (12). Different panels correspond to different normalized radii of curvature ranging from $\mathcal{R}_6 = 0.1$ to $\mathcal{R}_6 = 0.009$. Different symbols used to plot exemplary curves correspond to arbitrarily chosen values of shielding factor ranging from $\eta = 0.015$ to $\eta = 0.15$ (each curve represents the same shielding conditions η for all 102 pulsars considered).

The vertical line in Fig. 1 corresponds to PSR B0943+10 (N1=41 in Table 1), which was observed using XMM-Newton by ZSP05. Three horizontal lines correspond to T_s equal to about 2, 3 and 4 MK (from bottom to the top), respectively, calculated from equation (12). (More exactly, we marked $T_s = T_i = 2.08, 3.11$ and 4.14 for $B_s/B_q = 2.7, 4.8$ and 7.2 , respectively). Thus, the hatched areas encompassing these lines correspond to the range of surface temperatures $T_s \cong (3 \pm 1) \times 10^6$ K deduced observationally for the polar cap of B0943+10 from XMM-Newton observations (ZSP05, see their Fig. 1).

4.2. ICS-NTPSG model

Let us now consider the resonant inverse Compton scattering radiation model (ICS-NTPSG). The major difference between CR and ICS cases is the additional regulation of T_s caused by the condition $h \approx l_e$, where l_e is inversely proportional to T_s . In fact, the increase of the surface temperature causes the decrease of h , and hence, the decrease of ΔV . This makes the back-flow heating of the polar cap surface less intense. Let us estimate the surface temperature in the ICS dominated case. The average Lorentz factor of electrons or positrons can be estimated by the gap height and the partially screened potential drop as $\gamma = (1.1 \times 10^2) P^{1/6} \dot{P}_{-15}^{-1/6} b^{1/3} (T_s/10^6)^{2/3} \eta^{-1/3}$. Using the kinematic near threshold condition and the expression of the resonant ICS photons energy (see section 2) we get $\hbar\omega = (7.5 \times 10^{-8}) \gamma b (P \dot{P}_{-15})^{-1/2}$, which leads to another estimate for the average Lorentz factor $\gamma = 2.5 (T_s/10^6)^{1/3} \mathcal{R}_6^{1/3}$. Combining these two expressions for γ we find that for the case of the ICS dominated NTPSG the following relationship should hold $\eta = 8.14 \times 10^{-5} P^{1/2} \dot{P}_{-15}^{-1/2} b (T_s/10^6) \mathcal{R}_6^{-1}$. As a result, contrary to the CR case, the shielding factor η is not a free parameter in the ICS case, and the analysis similar to that presented in Fig. 1 is not relevant. However, we can use the quasi-equilibrium condition $\sigma T_s^4 = \gamma m_e c^3 n_0 \eta$, which leads to $T_s = (8.8 \times 10^4) \left(\gamma \eta b P^{-3/2} \dot{P}_{-15}^{-1/2} \right)^{1/4}$. Using the expressions of η and γ we can then obtain

$$T_s = (1.5 \times 10^4 \text{ K}) \mathcal{R}_6^{-1/4} P^{-3/8} \dot{P}_{-15}^{-3/8} b^{3/4}. \quad (16)$$

Consequently, we can obtain the expression for the shielding factor

$$\eta = (1.2 \times 10^{-6}) P^{1/8} \dot{P}_{-15}^{-7/8} \mathcal{R}_6^{-5/4} b^{7/4}. \quad (17)$$

Thus, for a given pulsar (P, \dot{P}) the values of T_s and η are determined by the parameters of the local surface magnetic field \mathcal{R}_6 and b . In Figure 2 we plot T_s as a function of B_s/B_q (Eq. [8]) for different values of \mathcal{R}_6 and η . The smooth lines in both panels correspond to the ion critical temperature, while other lines marked by different symbols shown in legends

correspond to the actual surface temperature calculated for the CR case (upper panel) and the ICS case (lower panel). We look for partially screened solutions corresponding to the intersection of smooth and symbol-broken lines.

As seen from the lower panel of Figure 2, equations (16) and (17) cannot be self-consistently satisfied. In fact, unlike in the CR case presented in the upper panel, in the ICS case the surface temperature $T_s \simeq 10^6$ K (Eq. 16) is considerably lower than T_i (Eq. 12). Bringing T_s close to T_i would imply $\eta = 1$ (pure vacuum), which is inconsistent with Eq. 17. Thus, if the pair creation is controlled by ICS, then the acceleration region should be a pure vacuum gap rather than a PSG. This is consistent with previous results of GM02, who concluded that in the pure vacuum gap case ICS seed photons are more efficient in driving the cascading pair production. However, GM02 failed to understand that CR pair production mechanism produces more polar cap heating and thus makes the gap partially screened. In such a case the ICS pair production still occurs but it is no longer the dominant mechanism to control the properties (height, potential drop, etc) of the acceleration region above the polar cap.

5. Thermal signatures of hot polar cap

Knowing that ICS cannot contribute significantly to the pair production process in a PSG, let us consider polar cap heating by back-flow plasma particles created from CR seed photons. Using the near threshold condition in the form $h = (4/3)(mc\mathcal{R}^2/\hbar\gamma^3) = h_3 10^3$ cm (see below Eq. [8]) we can rewrite equation (7) in the form

$$T_s = (7.7 \times 10^6 \text{ K}) P^{-2/7} \eta^{2/7} \mathcal{R}_6^{1/7} \left(\frac{B_s}{B_q} \right)^{2/7}. \quad (18)$$

Consequently, we can obtain efficiency of thermal X-ray emission in the form

$$\frac{L_x}{\dot{E}} = 0.15 P^{19/14} \dot{P}_{-15}^{-1/2} \eta^{8/7} \mathcal{R}_6^{4/7} \left(\frac{B_s}{B_q} \right)^{1/7}, \quad (19)$$

where $L_x = \sigma T_s A_{bol}$ is the X-ray luminosity from the hot polar cap with the surface area $A_{bol} = \pi r_p^2$ (Eq. [4]) and $\dot{E} = I\Omega\dot{\Omega} = 3.95 \times 10^{31} \dot{P}_{-15}/P^3$ erg/s is the spin-down power. For the twin radio pulsars PSR B0943+10 and PSR B1133+16 the X-ray signatures of the hot polar cap are $T_s \sim 3 \times 10^6$ K, $\dot{E} \approx 10^{32}$ erg/s and $L_x/\dot{E} \sim 5 \times 10^{-4}$ (see Table 1 in Paper I). Using these measurements we can infer from equations (18) and (19) an approximate condition in the form $\eta^2 \mathcal{R}_6 \sim 6.5 \times 10^{-5}$.

Figures 3 and 4 present calculations of the efficiency L_x/\dot{E} and the temperature T_s , respectively, for 102 pulsars from Table 1. One should emphasize that these calculations did not assume the existence of the PSG in the form $T_s = T_c$ (Eqs. [12] and [14]). Thus, these figures should be considered in association with Fig. 1, which takes into account the existence of the PSG. The vertical solid lines correspond to PSR B0943+10 for which $T_s = (3 \pm 1) \times 10^6$ K (corresponding to $B_s/B_q=4.8$ in Fig. 1) and $L_x/\dot{E} = (5 \pm 2) \times 10^{-4}$ (ZSP05). Due to weak dependence of the efficiency on the magnetic field we decided to use only one value of $B_s/B_q=4.8$ in Fig. 3 to avoid overlapping of too many lines. The observational range of L_x/\dot{E} and T_s are marked by the hatched belts in Figs. 3 and 4, respectively. Since L_x/\dot{E} in equation (19) depends on both P and \dot{P} we have sorted pulsars in Fig. 3 according to increasing value of \dot{E} , which are marked on the top of the figure (N2 in Table 1). If $L_x/\dot{E} \sim 10^{-3} \div 10^{-4}$ for all pulsars, then one can say that the shielding factor η should be larger for pulsars with larger \dot{E} . Also, it follows from Fig. 4 that if $T_s = (2 \div 4) \times 10^6$ K in all pulsars, then the shielding factor η should be larger for longer period pulsars. This is consistent with equation (A2) in Paper I, where $\eta \propto P/P_3$.

6. Special case of PSR B0943+10

As already mentioned above, both the subpulse drift rate and the polar cap heating rate (due to subpulse-producing sparks) are related to the same value of the accelerating

potential drop. In Paper I, we found a “clear cut” formula involving two observables: the X-ray luminosity L_x and the tertiary drift periodicity \hat{P}_3 , which is independent of details of the acceleration region (see Eqs. [1] and [2] in Paper I). This relationship holds perfectly for PSR B0943+10, which is the only pulsar for which both L_x and \hat{P}_3 values are available. In this pulsar $P = 1.09$ s, $\dot{P} = 3.5 \times 10^{-15}$, $P_3 = 1.86P$, $\hat{P}_3 = 37.4P$ and $N = \hat{P}_3/P_3 = 20$ (Deshpande & Rankin 1999, 2001). On the other hand, ZSP05 observed PSR B0943+10 with XMM-Newton and obtained a thermal BB fit with $L_x = 5 \times 10^{28}$ erg/s and $T_s \approx 3 \times 10^6$ K, corresponding to small polar cap with the bolometric surface area $A_{bol} \approx 10^7$ cm² (as compared with the canonical area $A_{pc} = 6 \times 10^8$ cm²). We can now compare the general results of Paper I with the specific calculations presented in this paper. According to equations (A1) and (A2) from Paper I, we have $\hat{P}_3/P = (r_p/h)(1/2\eta)$ and $\eta \approx (1/2\pi)(P/P_3)$. Thus in PSR B0943+10, the shielding parameter $\eta = 0.09$ and the complexity parameter $r_p/h = N/\pi = 6.36$, in consistency with Gil & Sendyk (2000, see also Gil, Melikidze & Mitra 2002). Let us analyze in this respect our Fig. 1, which allows to read off the physical parameters of the acceleration region for a given pulsar within a particular model η . For PSR B0943+10, only the intersections of the vertical lines corresponding to N1=41 (see Table 1) with the hatched belts, or even with the horizontal line $T_s = 3\text{MK}$, are relevant. The above value of $\eta = 0.09$ corresponds to the radius of curvature $\mathcal{R}_6 \sim 6.5 \times 10^{-5}\eta^{-2} \sim 0.009$ (see the condition below Eq. [19]), and thus from the lower-right panel of Fig. 1 we have $B_s/B_q \sim 5$ or $B_s \sim 2 \times 10^{14}$ G and $T_s \sim 3 \times 10^6$ K. These values are very consistent with the appropriate entry for PSR B0943+10 in Table 1 of Paper I.

Using the model values $\eta = 0.09$ and $\mathcal{R}_6 = 0.009$ obtained above we get from the lower-right panel of Fig. 3 that $L_x/\dot{E} = 5 \times 10^{-4}$ in PSR B0943+10, as observed (ZSP05). Thus, our detailed model calculations are perfectly consistent with the general formula obtained in Paper I (Eq. [2]), which gives $\dot{P}_3/P = (0.75)^{1/2}(L_x/\dot{E})^{-1/2} \sim 38$, as measured

by Deshpande & Rankin (1999, 2001). The middle curve in the lower-right panel in Fig. 4 is consistent with the model solution for PSR B0943+10, that is: $\mathcal{R}_6 = 0.009$, $B_s/B_q = 4.8$ ($B_s = 2 \times 10^{14}$ G), $T_s = 3 \times 10^6$ K and $\eta = 0.09$. This set of parameters can be also inferred from the upper panel in Fig. 2.

7. Discussion and Conclusions

The phenomenon of drifting subpulses has been widely regarded as a powerful tool for understanding the mechanism of coherent pulsar radio emission. RS75 first proposed that drifting subpulses are related to $\mathbf{E} \times \mathbf{B}$ drifting sparks discharging the high potential drop within the inner acceleration region above the polar cap. The subpulse-associated streams of electron-positron plasma created by sparks were supposed to undergo a two-stream instability which should lead to generation of the coherent radiation at radio wave lengths. However, both the calculations of the binding energy (critical for spark ignition) and the growth rate of the two-stream instability have suggested that neither the sparking discharge nor the two-stream instability proposed by RS75 were able to work in actual pulsars (for review see e.g. GM01). Nonetheless, qualitatively their idea is still considered very attractive, and the authors of this paper have been continuing efforts (GM01, GM02, GMG03) to search for mechanisms that would actually make the RS75 model to work. In this paper we present a self-consistent scenario that is based only on one assumption, i.e. the existence of a strong non-dipolar surface magnetic field at the polar cap region. This assumption seems to be quite well justified observationally and theoretically (see Urpin & Gil 2004, for short review).

In PSR B0943+10 the surface temperature T_s is about 3MK (ZSP05), which implies $B_s = bB_d \sim 2 \times 10^{14}$ G if one applies J86 theory (Eq. [12]) to this case. The value exceeding 10^{14} G may seem extremely high, but at least three radio pulsars have dipolar magnetic

fields above 10^{14} G (McLaughlin et al. 2003, and references therein). The non-dipolar surface magnetic fields could be even stronger. The reason that the inferred non-dipolar field is even stronger than in the pure vacuum case found in GM02 for the ICS seed photons is that we are using a lower binding energy calculations of Jones (1986), which are more robust than those of Abrahams & Schapiro (1991) (see Lai 2001, for critical review). However, generally the surface magnetic field required to form CR-NTVG (GM02) is still higher than that for CR-NTPSG obtained in this paper.

GM02 considered deviations from the blackbody conditions on the polar cap surface heated by spark. They introduced the so-called heat-flow coefficient $\kappa = Q_{rad}/(Q_{rad}+Q_{cond})$, which described the amount of heat conducted beneath the polar cap that cannot be transferred back to the surface during the spark development time scale (see Appendix B in GM02). The heat flow coefficient κ influenced the required surface magnetic field B_s in proportion to $\kappa^{0.57}$ (for CR case). GM02 argued that for $T_s \sim 1$ MK this effect could reduce the required B_s by a factor of about 2. However, if $T_s \sim 3$ MK as indicated by the case of PSR B0943+10, the reduction effect is negligible (factor 0.75 at most) and we ignored it in this paper.

Our analysis suggests the following picture of pulsars: In strong magnetic fields $B_s \sim 10^{14}$ G near the neutron star surface, the binding energy is high enough to prevent a full thermionic flow from the hot polar cap at the corotation limited level. A partially screened vacuum gap develops and the high acceleration potential drop just above the polar cap is discharged by a number of isolated electron-positron sparks. The polar cap surface is heated by back-flowing plasma particles to temperatures $T_s \sim 10^6$ K, just below the critical temperature T_c at which the thermionic flow screens the gap completely. The typical radii of curvature of the field lines \mathcal{R} is of the order of polar cap radii $r_p \sim 10^3 - 10^4$ cm. The only parameter that is thermostatically adjusted in a given pulsar is the shielding parameter

$\eta = 0.001(B_s/B_q)\mathcal{R}_6^{-0.5}P \sim 0.001T_6^{1.43}\mathcal{R}_6^{-0.5}P$, which determines the actual level of charge depletion with respect to the pure vacuum case ($\eta=1$), and in consequence the polar cap heating rate as well as the spark drifting rate. It is worth to emphasize that $\eta \sim 0.1$ for longer period pulsars $P \sim 1$ s and $\eta \sim 0.01$ for shorter period pulsars. Our calculations are consistent with PSR B0943+10 and a few other drifting pulsars, for which the signatures of X-ray emission from the hot polar cap were detected (Paper I).

Usov (1987) first pointed out that the non-stationarity associated with sparking discharges naturally leads to a two-stream instability as the result of mutual penetration between the slower and the faster plasma components. Asseo & Melikidze (1998) developed this idea further, calculated the instability growth rates, and demonstrated that Usov's instability is very efficient in generation of Langmuir plasma waves. Conversion of these waves into coherent electromagnetic radiation escaping from the pulsar magnetosphere was considered and discussed by Gil, Melikidze, & Pataraya (2000) and Gil, Lyubarski, & Melikidze (2004). The observed pulsar radiation was shown to be an indirect consequence of sparking discharges within the inner acceleration region just above the polar cap. In light of this paper we can therefore suggest that the coherent pulsar radio emission is likely conditional on the existence of strong non-dipolar surface magnetic fields at the polar cap, with strength about 10^{14} G and radius of curvature about 10^4 cm. We described properties of thermal X-ray emission from hot polar caps that should be detectable from nearby radio pulsars. In the accompanying Paper I we derived a clear-cut relationship between radio and X-ray signatures of drifting subpulses, while in this paper we unravelled physical conditions for which such a relationship should hold.

We acknowledge the support of the Polish State Committee for scientific research under Grant 2 P03D 029 26 (JG & GM) and NASA grants NNG05GB67G, NNG05GH91G and NNG05GH92G (BZ).

REFERENCES

Abrahams, A.M., & Shapiro, S.L. 1991, *ApJ*, 374, 652

Arons, J. & Scharlemann, E. T. 1979, *ApJ*, 231, 854

Asseo, E., & Melikidze, G.I. 1998, *MNRAS*, 301, 59

Becker, W., Trümper, J., 1997, *A&A*, 326, 682

Cheng A.F., Ruderman M.A., 1980, *ApJ*, 235, 576 (CR80)

Cheng K.S., Gil J., & Zhang L., 1998, *ApJ*, 493, L35

Daugherty J., Harding A.K., 1983, *ApJ*, 273, 761

Deshpande, A.A., & Rankin, J.M. 1999, *ApJ*, 524, 1008 (DR99)

Deshpande, A.A., & Rankin, J.M. 2001, *MNRAS*, 322, 438 (DR01)

Erber, T. 1966, *Rev. Mod. Phys.*, 38, 626

Gil, J., & Sendyk, M., 2000, *ApJ*, 541, 351 (GS00)

Gil, J., Melikidze, G.J., & Pataraya, A. 2000, *ApJ*, 544, 1080

Gil J., & Mitra D., 2001, *ApJ*, 550, 383 (GM01)

Gil J. & Melikidze G.I., 2002, *ApJ*, 577, 909 (GM02)

Gil, J., & Sendyk, M. 2003, *ApJ*, 585

Gil, J., Melikidze, G.I., & Mitra, D. 2002, *A&A*, 388, 246

Gil J., Melikidze G.I., & Geppert U., 2003, *A&A*, 407, 315 (GMG03)

Gil, J., Lyubarski, Yu., & Melikidze, G.I. 2004, *ApJ*, 600, 872

Gil, J., Melikdize, G.I., & Zhang, B. 2006, ApJ, submitted (astro-ph/0512653) (Paper I)

Goldreich P., & Julian H., 1969, ApJ, 157, 869 (GJ69)

Harding, A. K., & Muslimov, A. G. 1998, ApJ, 508, 328

Jones P.B., 1986, MNRAS, 218, 477 (J86)

Lai D., 2001, Rev. Mod. Phys., 73, 629

McLaughlin M.A., Stairs, I.H., Kaspi, V.M., et al., 2003, ApJ, 591, L135

Possenti A., Cerratto R., Colpi M., et al., 2002, A&A, 387, 993

Rankin J.M., 1986, ApJ, 301, 901 (R86)

Ruderman M.A., Sutherland P.G., 1975, ApJ, 196, 51 (RS75)

Urpin V., & Gil J., 2004, A&A, 415, 356

Usov, V. 1987, ApJ, 320, 333

Weltevrede P., Edwards R.I., & Stappers B.A., 2006, A&A, 445, 243

Wright, G. A. E. 2003, MNRAS, 344, 1041

Zhang B., Harding A., & Muslimov A., 2000, ApJ, 531, L135

Zhang B., Sanwal D., & Pavlov G.G., 2005, ApJ, 624, L109 (ZSP05)

Zhang, B., Qiao, G. J., Lin, W. P. & Han, J. L. 1997, ApJ, 478, 313

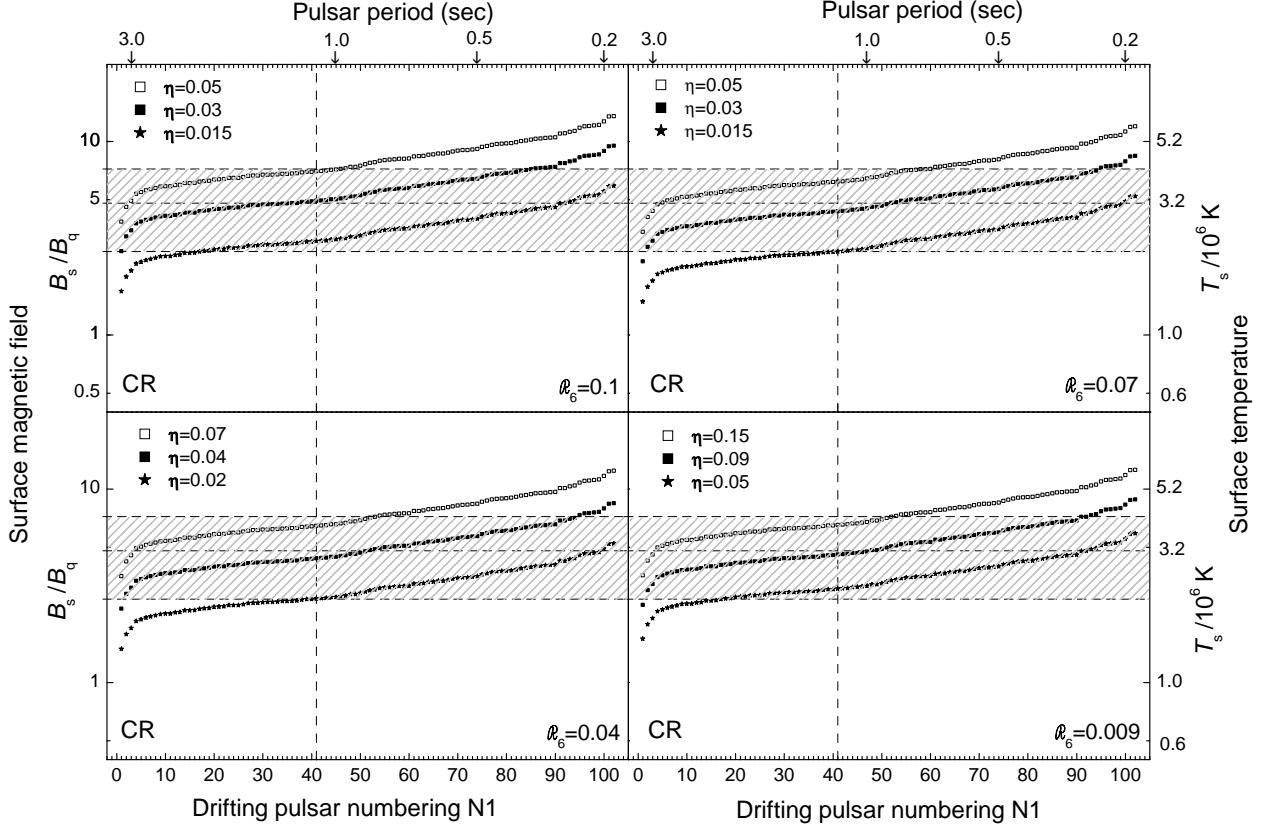


Fig. 1.— Models of partially screened inner acceleration regions (PSG) driven by curvature radiation seed photons above positively charged (ion case) polar cap for 102 pulsars from Table 1, sorted according to pulsar period. The horizontal axes correspond to the pulsar number $N1$ (bottom) or pulsar period (top). The vertical axes correspond to the surface magnetic field B_s/B_q (left-hand side), or surface temperature $T_s/10^6$ K (right-hand side). The calculations were made for conditions corresponding to very strong ($B_s > 5 \times 10^{12}$ G) and curved ($0.1 > \mathcal{R}_6 > 0.005$) surface magnetic field. The vertical lines correspond to the case of PSR B0943+10 ($N1=41$) and the hatched area encompassing three horizontal lines correspond to the range of surface magnetic field and temperature inferred for this pulsar from the XMM-Newton observation (ZSP05). These models allow to read off the physical conditions existing in the acceleration region above the polar cap of a particular pulsar in the form of parameters such as B_s , \mathcal{R}_6 and η .

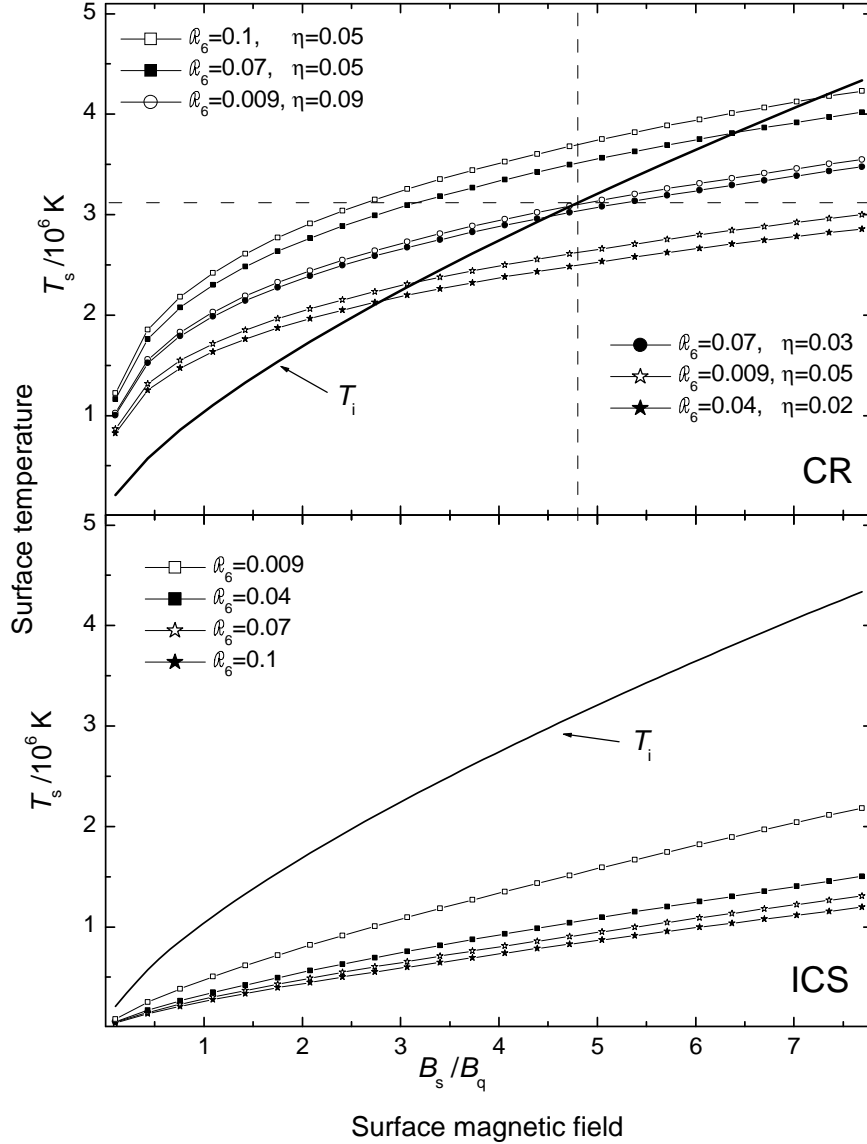


Fig. 2.— Dependence of the surface temperature on the surface magnetic field in the case of NTPSG for CR (upper panel) and ICS (lower panel) cases. Solid lines represent the critical ion temperature T_i , while the symbol-broken lines represent the actual surface temperature. As one can see only the CR case can work in pulsars with positively charged (ion case) polar cap. The solution for PSR B0943+10 is marked by the dashed lines ($B_s = 4.8B_q \sim 2 \times 10^{14}$ G, $\mathcal{R}_6 = 0.009$, $\eta = 0.09$ and $T_s = 3.1$ MK).

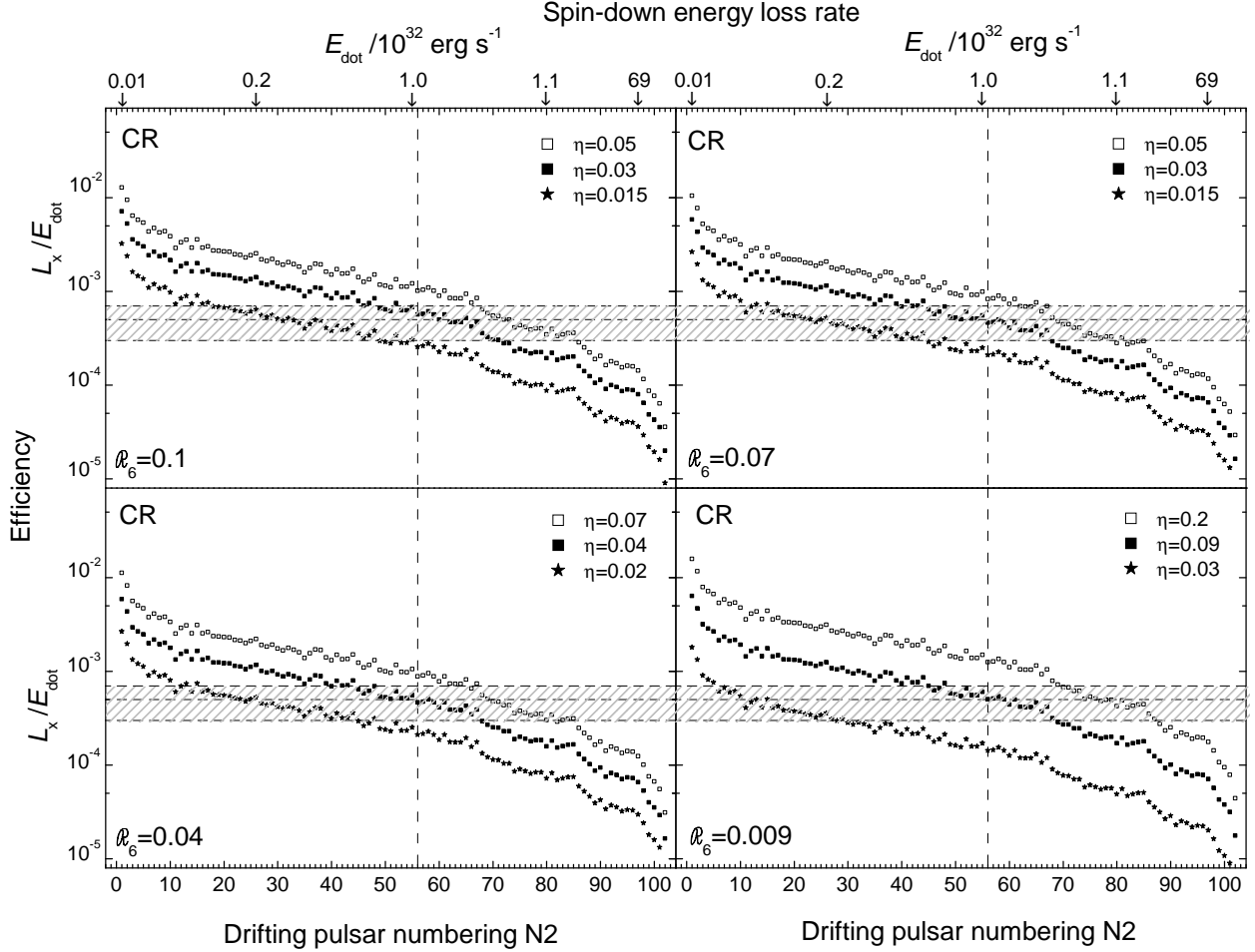


Fig. 3.— The thermal radiation efficiency from the hot polar cap for 102 pulsars from Table 1 for different parameters of the PSG marked in the legends. Pulsars are sorted according to the pulsar spin-down luminosity (N2 in Table 1). For clarity of presentation the surface field is fixed at $B_s/B_q=4.8$.

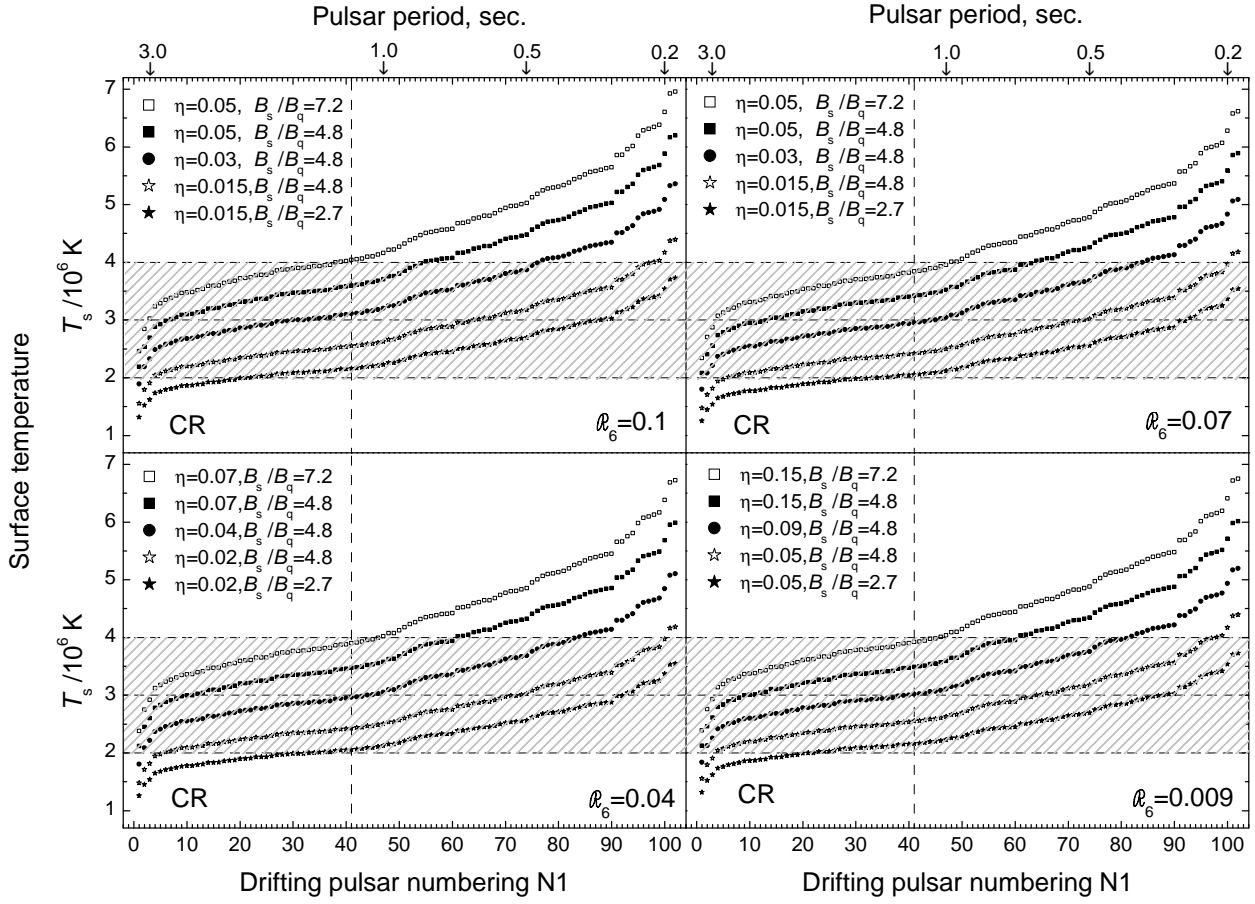


Fig. 4.— Surface temperature of hot polar cap for 102 pulsars from Table 1 for different parameters of the PSG marked in the legends. Pulsars are sorted according to the pulsar period (N1 in Table 1).

Table 1: List of 102 pulsars with drifting subpulses compiled from R86, GM02 and WES05. N1 and N2 refer to sorting according to pulsar period P and spin-down luminosity \dot{E} , respectively.

Name	N1	N2	Name	N1	N2	Name	N1	N2	Name	N1	N2
B0011+47	31	17	B0823+26	71	71	B1822-09	54	91	B1953+50	73	69
B0031-07	49	25	B0826-34	10	10	J1830-1135	1	11	B2000+40	50	53
B0037+56	40	50	B0834+06	28	60	B1839+56	15	18	J2007+0912	76	61
B0052+51	6	40	B0919+06	78	97	B1839-04	11	5	B2011+38	97	100
B0136+57	94	99	B0940+16	42	3	B1841-04	47	64	B2016+28	69	37
B0138+59	33	13	B0943+10	41	56	B1844-04	67	98	B2020+28	89	86
B0144+59	100	85	B1039-19	24	19	B1845-01	61	76	B2021+51	72	79
B0148-06	20	8	B1112+50	14	28	B1846-06	21	74	B2043-04	18	22
B0301+19	23	24	B1133+16	36	51	B1857-26	65	38	B2044+15	38	7
B0320+39	3	2	B1237+25	25	20	B1859+03	62	80	B2045-16	8	46
B0329+54	59	66	B1508+55	56	72	B1900+01	57	70	B2053+36	99	84
B0450+55	90	87	B1530+27	39	29	J1901-0906	12	16	B2106+44	81	44
B0523+11	87	48	B1540-06	60	54	B1911-04	52	68	B2110+27	35	47
B0525+21	2	35	B1541+09	55	41	B1914+13	93	96	B2111+46	46	32
B0540+23	95	101	B1604-00	80	65	J1916+0748	70	88	B2148+63	84	58
B0609+37	92	52	B1612+07	34	45	B1917+00	29	63	B2154+40	19	39
B0621-04	45	33	B1642-03	83	83	B1919+21	26	27	B2255+58	85	92
B0626+24	75	75	J1650-1654	13	30	B1923+04	43	49	B2303+30	17	34
B0628-28	30	62	B1702-19	91	95	B1924+16	68	89	B2310+42	88	55
B0727-18	74	94	B1717-29	64	59	B1929+10	98	90	B2319+60	5	31
B0740-28	101	102	B1737+13	53	57	B1933+16	86	93	B2324+60	96	81
B0751+32	22	21	B1738-08	7	14	B1937-26	82	73	B2327-20	16	42
B0809+74	27	4	B1753+52	4	6	B1942-00	44	23	J2346-0609	37	36
J0815+0939	63	26	B1804-08	102	67	B1944+17	77	15	B2351+61	48	77
B0818-13	32	43	B1818-04	66	82	B1946+35	58	78			
B0820+02	51	9	B1819-22	9	12	B1952+29	79	1			